ASTROBIOLOGY
Volume 4, Number 1, 2004

Research Paper

Meteor Wake in High Frame-Rate Images—Implications for the Chemistry of Ablated Organic Compounds

PETER JENNISKENS[1] and HANS C. STENBAEK-NIELSEN[2]

ABSTRACT

Extraterrestrial organic matter may have been chemically altered into forms more ameanable for prebiotic chemistry in the wake of a meteor after ablation. We measured the rate of cooling of the plasma in the meteor wake from the intensity decay just behind a meteoroid by freezing its motion in high frame-rate 1,000 frames/s video images, with an intensified camera that has a short phosphor decay time. Though the resulting cooling rate was found to be lower than theoretically predicted, our calculations indicated that there would have been insufficient collisions to break apart large organic compounds before most reactive radicals and electrons were lost from the air plasma. Organic molecules delivered from space to the early Earth via meteors might therefore have survived in a chemically altered form. In addition, we discovered that relatively small meteoroids generated far-ultraviolet emission that is absorbed in the immediate environment of the meteoroid, which may chemically alter the atmosphere over a much larger region than previously recognized. Key Words: Prebiotic chemistry—Origin of life—Meteors—Meteor wake—Temperature. Astrobiology 4, 95–108.

INTRODUCTION

INFALLING EXTRATERRESTRIAL MATTER has long been argued to be an important source of prebiotic molecules for the origin of life (*e.g.,* Ponnamperuna, 1981; Thomas *et al.,* 1997). Oró and Lazcano (1997) have discussed the long history of the field. Much effort has been made to identify prebiotic molecules in meteorites and interplanetary dust particles, which are available for study in the laboratory. In a new chapter to the story, we argue that the more important source of organic molecules is the meteoric matter ablated in the Earth's atmosphere (Jenniskens *et al.,* 2000a; Jenniskens, 2001). Ablation in the Earth's atmosphere is the fate of the bulk of infalling organic laden extraterrestrial matter (Ceplecha, 1992; Love and Brownlee, 1993). Because atmospheric chemistry in the meteor and ambient environment can chemically change those ablation products into forms more amenable for prebiotic chemistry, this can be a very significant process of relevance to astrobiology.

In an earlier paper (Jenniskens *et al.,* 2004a), we argued that much of the organic matter may leave the meteoroid in the form of relatively large compounds. This paper addresses the question whether ablated organic compounds can survive

[1]Center for the Study of Life in the Universe, SETI Institute, Mountain View, California.
[2]University of Alaska, Fairbanks, Alaska.

the chemistry with reactive species in the air plasma in a chemically altered but still reduced form. It has always been assumed that the organic matter is consumed by oxygen atoms to form CO_2 and water. However, the concentration of reactive species is time and temperature dependent. Hence, an important parameter for understanding the fate of exogenous organic matter is a knowledge of the cooling rate of the plasma, especially in the wake of relatively small meteoroids of size ~150 μm at the peak of the mass influx curve (Ceplecha, 1992; Love and Brownlee, 1993).

Our current understanding of how meteors deposit cometary and asteroidal material in the atmosphere and how its chemical composition is changed during ablation and subsequent chemistry in the air plasma in the wake of the meteoroid is primarily based on spatially unresolved optical and radar observations (Öpik, 1958; Bronshten, 1983; Ceplecha *et al.,* 1998). Immediately behind the meteoroid, an air plasma is created by air molecules that are accelerated by colliding with the meteoroid and its ablation vapor cloud, and decelerated by subsequent collisions with the ambient air environment. Order of magnitude estimates on the rate of elastic and inelastic collisions within the air plasma are obtained from measurements of the trail width (Öpik, 1958; Hawkes and Jones, 1978). In contrast, the loss of translational energy in the wake of meteoroids has recently been calculated using a Direct Monte-Carlo Simulation model that described the rarefied flow around a 1 g Leonid (Boyd, 2000; Popova *et al.,* 2000; Jenniskens *et al.,* 2000a). That model predicts a time-dependent temperature ($T \sim t^{-1/2}$) from about 6,300 K at 10 m behind the meteoroid to 3,400 K at a distance of 40 m. The new model shows that the ablation vapor cloud (due to molecules and atoms sputtered off, surrounding, and traveling with the meteoroid) determines to a large extent the size of the wake by dramatically increasing the collision cross section of the meteoroid.

While the process of excitation in suprathermal collisions implies a lack of thermodynamic equilibrium, the typical air plasma vibrational and electronic excitation temperatures and chemical equilibrium temperatures measured for such meteors all suggest T ~4,300 K, a value surprisingly independent of meteoroid mass and speed (Jenniskens *et al.,* 2004b).

This paper deals with the temperature decay following that excitation. The wake of actual meteors is complicated by unknown infrared and ultraviolet radiative cooling mechanisms, nonequilibrium chemistry in the meteor wake (Park and Menees, 1978), fragmentation of the meteoroid (Hawkes and Jones, 1978; Murray *et al.,* 1999; von Zahn, 2001), and by fragments ejected at high speed from a spinning grain (Le Blanc *et al.,* 2000; Taylor *et al.,* 2000).

Until now, the only useful measurement of the temperature decay in the meteor wake was that by Borovička and Jenniskens (2000), who discovered an afterglow of cooling meteoric plasma in the wake of a bright Leonid fireball, with a cooling time much slower than predicted by the Monte-Carlo Simulation model. In at least one part of the meteoroid trajectory, the afterglow was associated with secondary ablation from solid debris detected by way of spectroscopic evidence.

Measurements of meteor afterglow in fainter meteors are hampered by motion blurring and overexposure. In conventional imaging, the rapid motion of the meteoroid blurs all morphological detail. Instantaneous photography using rapidly rotating shutters has detected meteor wake out to ~150 m behind the meteoroid (Halliday *et al.,* 1980), but it is not very sensitive and is limited to meteors so bright that they do not characterize the typical rarefied flow conditions of small meteoroids. Moreover, instantaneous photography does not provide the high temporal resolution that can be achieved with today's high frame-rate imagers.

Here, we report high frame-rate imaging of a relatively faint −3 magnitude Leonid meteor from a ground location during the 2001 Leonid Multi-Instrument Aircraft Campaign (MAC) (Jenniskens and Russell, 2003). The most striking aspect of the images is the unexpected development of a bow-shock-like structure and a spherical luminosity before the shock, which is discussed elsewhere (Stenbaek-Nielsen and Jenniskens, 2003). This paper discusses the wake in the meteor images.

METHODS

The observations were made at the University of Alaska's Poker Flat Research Range 30 miles northeast of Fairbanks, AK (65.12N, 147.46W, and 0.39 km altitude) with an intensified charge coupled device (CCD) camera operating at 1,000

frames/s. The intensifier used was sensitive to light in the wavelength range ~500–900 nm with peak sensitivity at ~700 nm, where strong atomic line emissions of oxygen and nitrogen and the First Positive band emission of N_2 are present in meteor spectra. The intensifier phosphor had a brief decay time constant of 0.8 ms, ideally suited to study the natural afterglow in rapidly moving targets.

The CCD images were 256 × 256 pixels with 256 gray levels (8 bits) and 6.4 × 6.4° field of view. To facilitate the high frame rate, each image quadrant was read out in parallel through separate electronics. Because of small unavoidable differences between the four-quadrant electronics, some differences in intensity were expected to be visible in the images.

At 1,000 frames/s, gray level 255 was reached at a surface brightness of 3 Mega-Rayleigh (at 700 nm), which is about 25% of the CCD well depth. To further prevent blooming of the images, the gain of the intensifier was set for saturation to occur only at a higher brightness level. Images were continuously entered into the high-speed imager (HSI), which was equipped with a 4,000-frame circular digital buffer (*i.e.,* the buffer can contain 4 s of data). Upon recognizing an event, the operator would then intervene and save a selected sequence of the buffer to the computer disk storage.

The HSI was bore-sighted with a conventional wide-field low-light-level TV system, which provided a more classical video image of the meteor and a larger star field for orientation purposes. This system also consisted of an intensified CCD, but with a ~50 ms phosphor decay time, and the data were recorded on videotape with standard NTSC resolution (59.94 interlaced fields/s and a vertical resolution of 525 horizontal lines). Global Positioning System time was encoded on each field. The field of view was 21 × 16°, and the intensifier responded to wavelengths of 400–800 nm.

RESULTS

On the night of November 18 universal time (UT), 2001, the weather was mostly clouded. After 10 UT the eastern sky cleared. Near 10:20 UT a persistent meteor train was recorded on the wide-field imager for almost 20 min. At 10:42:59 UT, a bright Leonid meteor passed through the field of view of both imagers. This was close to the peak of the Leonid storm at ~10:40 UT, which was caused by Earth's crossing of the 1767 dust trail of comet 55P/Tempel-Tuttle (Kondrat'eva and Reznikov, 1985; Jenniskens, 2003).

The wide-field imager

The wide-field imager captured most of the meteor (Fig. 1), which moved from the bottom to the top across the central part of the 21 × 16° wide field over 29 frames (a little less than 1 s). The spatial resolution of the wide field camera was fairly similar to that of the HSI, which covers the central 6.4 × 6.4° of the field. However, the frame rate was lower, and the meteor moved significantly across each frame during the exposure. Also, the bright emissions caused the detector to saturate and "bloom." These effects combined to make it impossible to resolve any of the structures within the head of the meteor. A haze or thin clouds was present in the wide-field images. For ground-based observations at maximum instrument gain, and with a clear transparent dark sky, we would expect to see stars up to magnitude approximately +8.5. The limiting stellar magnitude in the images was slightly less than +7. A persistent train would have been much brighter, but it was not detected.

The meteor in the narrow-field HSI

Figure 2 shows representative frames acquired from a 400-ms HSI sequence of this event. Each image revealed an 0.94 × 0.94° section of the original 6.4 × 6.4° image centered on the meteor. The meteor entered the field of view at frame 60 within the sequence. The meteor was initially a point source, saturated at the center and slightly broader than the unsaturated star images, with only a faint trace of wake. The onset of subsequent features was gradual. The selected frames in Fig. 2 are those in which a new feature is well pronounced. Around frame 170, two unresolved lines developed at the tail of the meteor, which grew around frame 235 into a distinct spatial structure reminiscent of a shock front. Initially, only a diffuse triangular-shaped wake was visible between the two fronts (frame 200). Around frame 235, a wake developed inside the shock front that persisted for a relatively long time. At the same time, the meteor brightness increased dramatically. The emission on the outside of the "shock" structure gradually brightened, filling an almost perfect circle of light with a piece cut out (to which we will refer as the "bite-out"). At the

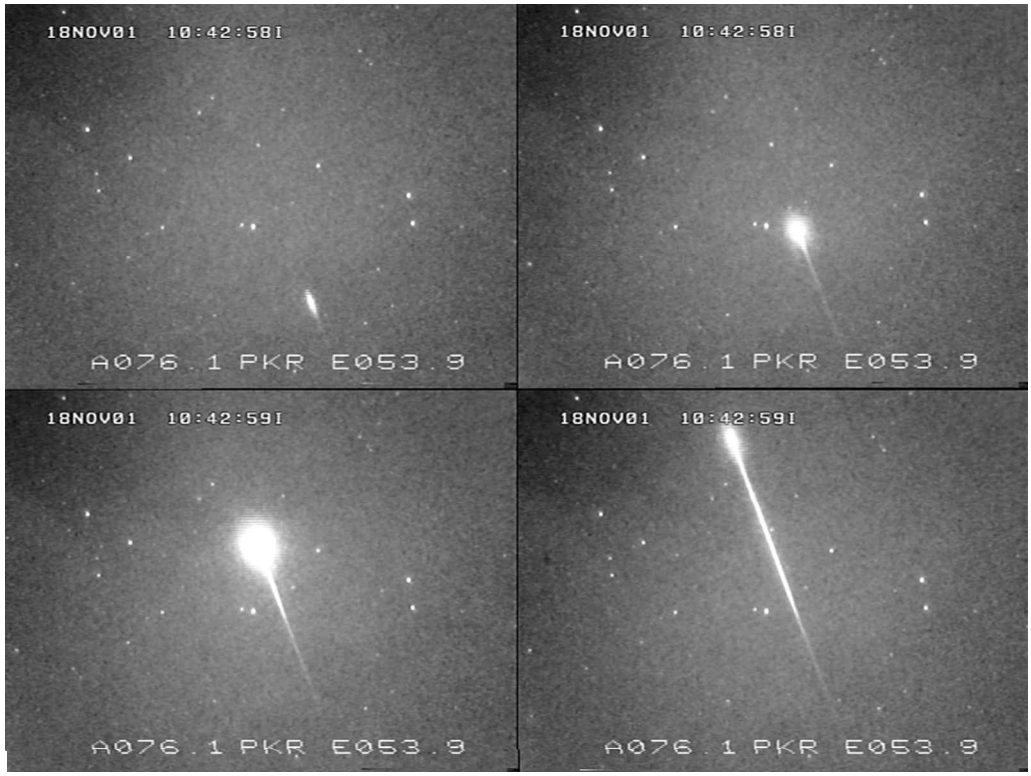

FIG. 1. Conventional intensified TV images of the event. The field of view is 21 × 16°, and the HSI (Fig. 2) covers the central portion of the field. The first image shows the meteor just before it entered the HSI field of view. The two next are within the HSI field of view, and the last just after the meteor exited the HSI field of view.

same time the "shock" opened up to about 45°. The structure was fully developed around frame 330. This is the first time such spatial structure has been reported. The HSI recording ended at frame 463.

The spatial structure was not the result of optical reflections in the camera. We noted that the images were already distinctly asymmetric when the meteor passed very close to the optical axis of the camera (frame 300), where any instrumental distortion of light would be expected to be symmetric. We did, however, find evidence of scattered light. Centered on the meteoroid position there appeared to be an underlying diffuse glow that was much wider than any spatial structure observed in the images. This diffuse glow may have been scattered light by thin clouds in the field of view.

The centers of the images were saturated. However, the blooming of the brightest part remained modest throughout the exposure period, and was much less than the observed spatial structure. This implies that the intensity of the meteor at its peak was at most a factor of a few brighter than the saturation level.

The wake

Following the images, with a small delay, was a wake of emission that persisted over the duration of the exposure. The characteristic delay identified this wake as being caused by the forbidden green line emission of O I at 557 nm (Halliday, 1958b; Baggaley, 1976, 1977). That O I wake was clearly seen as well in the TV imager (Fig. 2), where it remained visible for about 2 s.

A second wake phenomenon became visible at lower altitudes, which was identified (as discussed below) as the meteor afterglow resulting from collisional excitation of metal atoms and air plasma compounds (Halliday, 1958a; Borovička and Jenniskens, 2000). This feature was first seen around frame 300, and is a tail of emission growing from the saturated part of the meteor image. If this tail was due to phosphor decay from overexposure of the meteor, then there would have been an increase in blooming, which was not observed. Indeed, the tail faded slower than expected for an overexposed phosphor.

We conclude that during the development of the tail the meteor did not brighten enough to

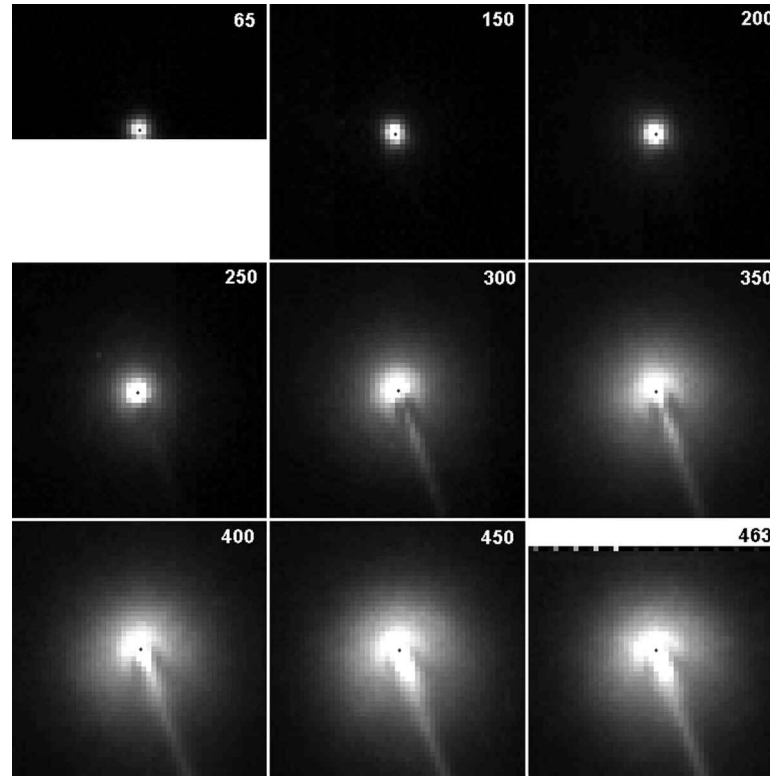

FIG. 2. Sections of the original high frame-rate images. Each is a 0.94 × 0.94° section from an original 6.4 × 6.4° image, which shows the development of the meteor morphology. The images were recorded at 1,000 frames/s. The frame number within the sequence is shown in the upper right corner. The calculated position of the meteoroid (see text) is shown by a dot.

overexpose the phosphor. The meteor did not leave what is called a persistent train, a chemiluminescence from the catalytic recombination of oxygen atoms and ozone molecules, which would be expected if the Leonid meteor had been brighter than magnitude −4 (Jenniskens *et al.,* 2000b). Such persistent trains have peak emission in the center of the system's response curve and are characterized by an apparent brightness of approximately +4 magnitude at this spatial resolution (Jenniskens *et al.,* 2000c).

ANALYSIS

Geometry of the observations

Both data sets had a sufficient number of stars distributed across the images to permit good spatial calibration. Using computer routines developed for analysis of image data in connection with auroral research (Stenbaek-Nielsen *et al.,* 1984), stars in the Smithsonian Astronomical Observatory star catalog were overlaid and fitted to the stars present in the images. The fitting program is interactive and can accommodate various display formats as well as nonlinearity associated with the optical system used in the imager. The resulting star fit provided directional information for all pixels within the individual images.

The center location of the meteor in each image was measured for all images in the HSI and the wide-field video data sequences. A computer program was written to calculate the location of the meteor in each image within the two image sequences using a fixed meteoroid velocity vector and an initial starting point derived from the meteor location in one of the early HSI images. The motion across the field depends upon the meteoroid angular velocity, the assumed range to the selected initial point, and, to a lesser degree, the radiant.

The meteoroid's velocity vector, given by the Leonid shower radiant position measured at the same time in Arizona by multistation photography in a Leonid MAC-related effort, was 154.1 ± 0.2° right ascension and 21.4 ± 0.1° declination (H. Betlem, personal communication). The speed was 71.6 ± 0.4 km/s, which is sufficiently high so that changes due to the Earth's gravitational field could be neglected. At the time of the event, 10:42:59 UT, the radiant was at 86.5° azimuth (east of north) and 22.3° elevation. The camera orientation was 76.1° azimuth and 53.9° elevation, resulting in an angle between camera orientation

and the velocity vector varying from 28° to 33° across the field of view. Thus, structures along the trajectory in the images were foreshortened by roughly a factor of 2. The pixel size in the high-speed images is 0.025 × 0.025. At a range of 135 km (altitude of 110 km), the spatial resolution was 57 m/pixel. This corresponds to the distance traveled by a meteor during the time its image on the phosphor screen fades by a factor *e*. With the meteor trajectory at an angle of 30° to the line of sight, the 1-pixel resolution along the trajectory was 114 m. In 1 ms the Leonid moved 72 m. Thus the meteor moved less than 1 pixel between frames, and the phosphor intensity decayed by 86% from one pixel to the next. Consequently, there was little "smearing" of spatial structures due to the motion of the Leonid meteor.

The calculated positions were fitted to the observed positions by adjusting the assumed range to the initial point and the Leonid velocity vector. A very good fit was obtained for a right ascension of 154.0° and a declination of +21.4°, which is in agreement with the position measured photographically. A small systematic deviation of 1 pixel in the *y* direction later in flight was due to the difficulty of choosing the center of the image once the "shock" forms. Indeed, the differences between calculated and observed positions in both data sets (Fig. 3) were similar to the accuracy by which the center could be determined, and hence the analysis showed the meteoroid velocity was constant during the time covered by the optical observations. This finding agrees with Spurný *et al.* (2000), who reported that the deceleration of similar Leonid meteors was below measurement accuracy in photographic data.

The positions for selected frames of the high frame-rate imager are given in Table 1. The meteor entered the wide field of view camera at an altitude of 122.9 km. It brightened very rapidly in the next two frames. The meteoroid entered the HSI field of view at an altitude of 115.6 km (frame 65). The bow shock and wake started to develop at about 110.4 km. The final HSI image, with the shock fully developed, was at 104.4 km when the meteor brightness started to level off. A larger fraction of the path was recorded in the wide-field TV imager, which showed that the meteor had a broad maximum in luminosity centered at an altitude of 100.6 km, after which the meteor decreased in intensity. It left the TV camera field of view at an altitude of 95 km, when it was still of magnitude +1. The position analysis is relatively insensitive to the assumed meteor velocity since varying the assumed range to the initial point can compensate for any error in velocity, within a reasonable range. For example, if the velocity decreased by 1 km/s the altitude of the path would decrease by ~2 km.

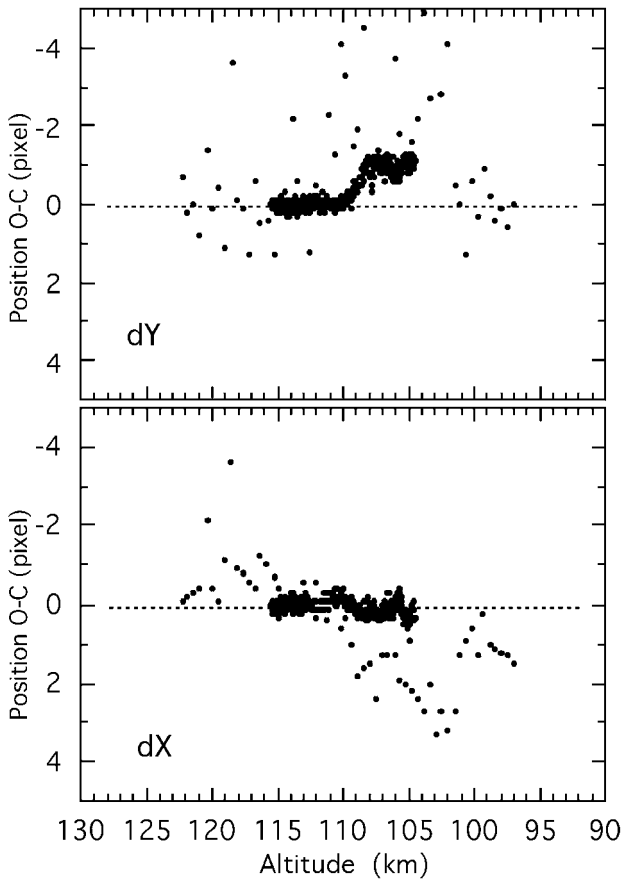

FIG. 3. Differences between observed and calculated positions of the meteor image center. The meteor crossed the field from the bottom to the top, and hence *dy* is essentially the difference along the track, while *dx* is the cross track difference. The abscissa is the altitude derived for each frame, while the ordinate is pixels. The observed center for the high frame-rate images was estimated to an accuracy of 0.2 pixels, while the TV record has an accuracy of about 1 pixel.

Relative brightness

The meteor's light curve (Fig. 4) was derived from the integrated intensity of both the HSI and TV images. Both data sets were processed differently in response to the amount of blooming, with overall good agreement to within 0.5 magnitudes. The HSI data in Fig. 4 show the integrated intensity over an area of 21 × 21 pixels centered on the position of the meteoroid. This covered the

TABLE 1. OBSERVED AND CALCULATED POSITIONS OF THE METEOR IN THE HSI DATA

	Calculated		*Observed*					
Frame	x	y	x	y	*Range*	*Latitude*	*Longitude*	*Altitude*
65	155.2	1.4	155.2	1.4	149.3	65.281	−145.492	115.6
100	148.8	18.8	148.9	18.8	147.1	65.280	−145.541	114.6
150	139.6	44.6	139.6	44.6	144.0	65.279	−145.610	113.2
200	130.0	71.4	129.9	71.5	140.9	65.279	−145.679	111.8
250	119.8	99.6	119.8	99.6	137.8	65.278	−145.749	110.4
300	109.0	129.4	109.2	129.0	134.8	65.277	−145.818	109.0
350	98.0	161.0	98.1	159.8	131.7	65.276	−145.887	107.6
400	86.2	193.2	86.5	192.0	128.7	65.275	−145.957	106.2
450	74.0	227.0	74.3	225.7	125.8	65.274	−146.026	104.8
463	70.8	235.8	71.1	234.7	125.0	65.274	−146.044	104.4

x,y are pixel location in the images, with (0,0) in lower left. The range is in km from the camera location, while latitude and longitude are in geographic degrees N and E. Altitude is in km.

meteor head, but not much of the tail. It did not include intensity lost in the central saturated pixels, but added intensity from the spatially extended component and the diffuse scattered light. The TV data were integrated over a 65 × 71 pixel rectangle that covered the full size of the bloomed area. Saturation effects were corrected for by treating the measured intensity as an optical depth. In the video, there is a substantial background signal, which was subtracted by computing the average signal in two similar-size rectangles located on either side of the meteor. To increase its temporal resolution, we measured at the beginning of data collection the intensity variation across the meteor images in each 1/30 s exposure while the blooming was still modest (solid line in Fig. 4). Each data set was calibrated to the *V* magnitude of the stars in the field of view over the range $V = +3.1$ to $+6.1$ magnitude. For similar cameras, it was found that blooming offset the effects of saturation over a much wider magnitude range, the relationship between blooming and saturation being close to that expected if the electron production is linear with incident light but the electrons distribute over more pixels: $V = \sim 2.5 \log \Sigma I_{\text{pixel}}$ (Jenniskens, 1999). Indeed, the expected intensity in the central pixels of the HSI was not much above the measured level, thus explaining the lack of blooming. The slightly higher brightness may reflect the fact that the HSI imager is sensitive to wavelengths longer than the *V* band, which overestimates the brightness in the calibration procedure. However, the limited number of calibration stars introduces a similar systematic uncertainty.

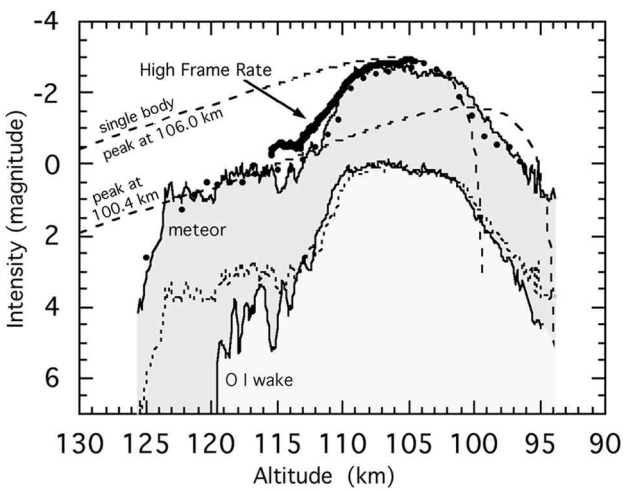

FIG. 4. Light curve of the meteor and its OI wake emission, derived from the integrated images (•) and from tracings across individual images (solid line). Dashed lines are classical light curves for a single solid body with peak intensity at different altitudes. The wake follows the meteor light curve between 115 and 97 km, but is 2.8 magnitudes fainter, as demonstrated by the dotted line, which is the meteor light curve shifted by +2.8 magnitudes.

At the peak of its brightness, the meteor had an absolute magnitude (*i.e.*, as seen from a distance of 100 km) of -2.7 ± 0.4 magnitude. Indeed, a meteor of this brightness would not have a bright persistent train. Other Leonid meteors of −2.7 magnitude have their peak brightness at 97 ± 4 km, in agreement with the value of 100.6 km found here (Jenniskens *et al.*, 1998; Betlem *et al.*, 2000). On video records with limiting magnitude approximately +6, such Leonids are usually detected first at altitudes of ~143 km, but their brightness does not increase to the photographic limiting magnitude of about +1 until they decend

to 118 ± 4 km, which coincides with the rapid brightening of the Leonid reported here. Both video and photographic records showed that the end point of the meteoroid trail was at 91 ± 3 km altitude, in good agreement with the altitude at which our Leonid meteor reached the photographic limiting magnitude of +1. Hence, a different wide-field camera would not have detected the meteor much beyond the frame of the current camera field.

Light intensity decay in the meteor wake

For each of the final frames 460–463, we subtracted the dark offset and the scattered light component. The latter was found from a perpendicular scan over the calculated position of the meteoroid. That scan is composed of a Lorentzian (full width at half-maximum = 0.04 pixel/155 intensity units) and Gaussian profile (σ = 0.03 pixel/125 intensity units). We assumed that the latter represented the spherical intensity halo with the bite-out from what appears to be a shock, and the former due to scattered light. We fitted the Lorentzian component to the front part of each trace, and found the peak to coincide to ±150 m with the calculated position of the meteoroid. After subtraction of this Lorentzian-shaped scattered light contamination, the result was divided by the brightness of the meteor when it was at that position (Fig. 4) to obtain the decay of light intensity over time.

The ratio of the final divided by the initial light intensity is plotted in Fig. 5, bottom trace (0.01–0.33 s), on a log-log scale. The graph shows two regimes of light decay, the first being a continuous decay from 0.01 to 0.09 s. This decay does not have a single $1/e$ time scale, but can be described by two $1/e$ decay times of 6.5 ms (0.01–0.04 s) and 25 ms (0.04–0.09 s). Recall that the decay time of the intensifier phosphor is 0.8 ms, a significantly smaller value. After 0.1 s, there was a gradual increase of intensity with time, rather than a decrease.

The cause of the two regimes of intensity decay could be identified from low resolution spectra of similar Leonids obtained during the 2001 Leonid MAC mission (Fig. 6). Two components are recognized in these spectra: (1) a delayed green-line (557 nm) emission of O I, and (2) a wake of emission similar to that of the main meteor that persisted for 1–2 frames, or <0.06 s. The emission of Na I, with a low upper energy level of 2.10 eV, persisted longer than the transitions

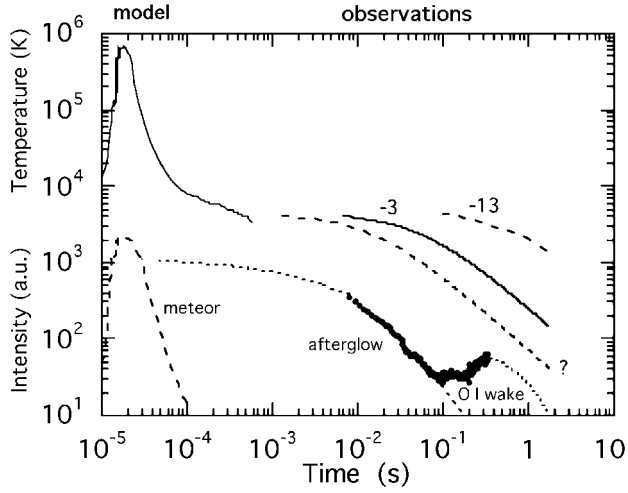

FIG. 5. Decay of light intensity and temperature behind the meteor. Data for $t < 0.0006$ s are from the model by Boyd (2000). Observations reported in this paper are shown as a dark band. The solid line above is the inferred temperature decay of the meteor vapor (marked "−3"). Results from Borovička and Jenniskens (2000) for a −13 magnitude fireball afterglow are also shown. The dashed line marked by a question is an extrapolated result for small meteoroids that is perhaps most relevant to the delivery of organics in the origin of life.

from higher energy states of Mg I (5.11 eV), the First Positive band of N_2 (7.2 eV), O I (10.7 eV), and N I (11.8 eV).

This pattern is the same as the one found by Borovička and Jenniskens (2000), who discovered a meteor afterglow in a −13 magnitude Leonid fireball, ascribed to secondary ablation. The new results are the first confirmation that meteor afterglow is a phenomenon present in relatively faint meteors.

Borovička and Jenniskens (2000) found that the decay of line intensities depends on the excitation potential, rather than on the transition probability. The intensity decay is therefore due primarily to the decrease of temperature rather than density. We can use this property to calculate the temperature variation from 0.01 to 0.09 s after passage of the meteoroid.

Borovička and Jenniskens (2000) found also that the exponential decay rate (B), defined as $I(t) \sim \exp(-B\ t)$, of light intensity (I) of a given transition depends linearly (factor D) on the excitation potential for most lines (E):

$$B = B_o + D\ E \qquad (1)$$

In our case, the observed intensity decay is a sum from the different components. However, at

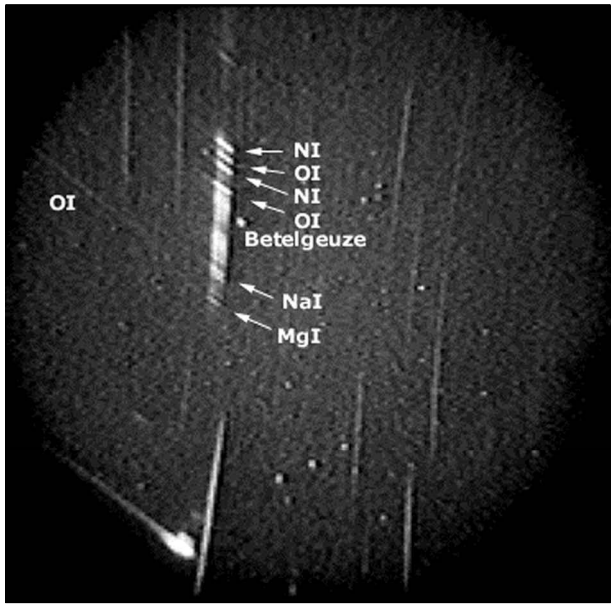

FIG. 6. Slit-less low-resolution spectrum of a −3 magnitude Leonid at 08:45:31 UT, November 18, 2001. There is delayed emission of the O I green line, and an afterglow of Mg, Na, O I, N I, and N_2. The meteor moved from left to right against a backdrop of stars in the constellation of Orion. The emission lines in the first order spectrum are elongated because of the meteor motion during the 1/30 s exposure.

least two contributions from transitions with quite different decay rates are needed to explain the observed decay of intensity. The two measured $1/e$ decay rates correspond to $B = 153$ and $B = 40$ s^{-1}, respectively. The spectral response curve of the HSI covered the range 400–800 nm, which included Mg I, Na I, N_2, and O I. Hence, the shallow slope of the decay rate plot is most likely the response from sodium, with $E = 2.1$ eV. The initial steep decline is most likely due to the First Positive band of N_2, but may have a contribution from O I (774 nm) and the much fainter Mg I line. If due to N_2, then $D = 22.1$ s^{-1} eV^{-1} and $B_o = -6.5$ s^{-1}, and if due to O I, then $D = 13.1$ s^{-1} eV^{-1}, $B_o = +12.4$ s^{-1}.

We adopt $B_o = 0$ s^{-1} (no production or destruction of emitting compounds) and $D = 19$ s^{-1} eV^{-1}. The calculated time dependence of the temperature of the meteoric vapor follows from Borovička and Jenniskens (2000):

$$5{,}040/T(t) = 5{,}040/T(t = 0) - D \times t \qquad (2)$$

The result for $T(t = 0) = 4{,}500$ K is shown in Fig. 5 and is compared with that calculated by Borovička and Jenniskens (2000), who had $D = 1.5$ s^{-1} eV^{-1}, a factor of 10 smaller. This earlier result pertains to a −13 magnitude fireball at 84 km altitude and predicts correctly the temperature of ~50 K, which was measured several minutes later in the persistent train of a similar bright fireball by LIDAR (LIght Detection And Ranging) resonance scattering of Doppler-broadened sodium (Chu *et al.*, 2000). We conclude that D is either a steep function of the peak brightness of the meteor or the rate of mass loss at the position of the measured afterglow.

DISCUSSION

Slowing down the loss of translational energy

The inferred rate of cooling is much slower than predicted in the model by Boyd (2000), shown on the left side of Fig. 5. Boyd (2000) calculated the translational temperature for a rarefied flow field around a 1-cm meteoroid at 95 km altitude (close to the ~0.4-cm meteoroid studied here at an altitude of 105 km). The calculations were performed for a grid that extended 40 m behind the meteoroid, representing times $t <$ 0.0006 s. The calculated temperature decays according to $T(t) \sim t^{-1/2}$, perhaps falling off more rapidly in exponential form at the end of the grid.

The disagreement between the model and observations is also apparent when one considers the expected intensity from the model plasma. The expected intensity of a local thermodynamic equilibrium (LTE) plasma is proportional to $I \sim \exp(-E/kT)$, where E is the excitation level of the upper state of an excited compound. For the relevant $E \sim 7.2$ eV, the predicted line intensity is the dashed line marked "meteor" in Fig. 6. The emission is expected to peak sharply a few mean-free paths (~1 m) from the position of the meteoroid at a time $t \sim 2 \times 10^{-5}$ s, where the (non-LTE) translation temperature is at its peak of $\sim 4 \times 10^6$ K, representative of a mean root mean square molecule velocity of 0.5 times the impact speed. However, that would have created a more point-like meteor with a strong blooming at the meteoroid position. The dashed line on Fig. 6 shows the probable emission distribution without effects of blooming subtracted from the HSI images. We note that this more gradual intensity decay favors the cooler LTE part of the temperature curve and can perhaps help explain the low

$T \sim 4{,}300$ K in meteor spectra (Jenniskens *et al.*, 2000a).

The role of meteor debris

Having established that something slows down the loss of translational energy or kinetic temperature of the meteor plasma, the question arises as to what is responsible for this effect. McCrosky (1955) first suggested that the luminosity of the wake is caused by the ablation of minute particles, which become detached from the meteoroid and lag behind it. However, Öpik (1958) criticized this idea because very small particles vaporize before falling far enough behind to provide an explanation for the observed length of the wake in bright fireballs (Bronshten, 1983). Also, Halliday (1958a) pointed out that changes in the luminosity of the wake are intimately linked to changes in the luminosity of the meteor, with no noticeable lag more than 0.01 s. This demands a rapid deceleration of the responsible agent. And, finally, the H and K lines of Ca^+ were detected in the wake of a bright fireball (with a peculiar V-shape splitting), which would demand collisions powerful enough to ionize calcium (6.1 eV), which are lacking in the thermal vapor of evaporating fragments.

Instead, Halliday (1958a) argued that any mixture of meteoric atoms and air will tend to slow down gradually, relative to the ambient environment in the wake of the meteor, and consideration of conservation of momentum shows the relative speed to be on the order of 5 km/s after 0.01 s. In this scenario, the afterglow phenomenon would be caused by the collisional excitation of meteoric metal atoms and air plasma until these compounds have slowed down.

Indeed, Borovička and Jenniskens (2000) measured at least one trail segment in a meteor afterglow that descended at a rate of ~2 km/s at 0.2 s. However, that same trail fragment also had $B_o > 0$, indicative of secondary ablation. Other trail segments did not move after formation, or show secondary ablation. Of course, meteoroid fragments can survive longer than envisioned by Öpik (1958) if they are in the wake of the meteoroid or its vapor cloud, or if they are rapidly decelerated by induced backward motion during fragmentation.

There is other evidence that links the afterglow phenomena to meteoroid fragmentation. The rapid increase in brightness at the beginning of the meteor's trajectory may signify a fragmentation that increased the effective surface area of the meteor vapor cloud. The increase was much more rapid than predicted for a classical light curve of a single solid body (dashed lines in Fig. 4). After that, the vapor cloud seemed to remain constant, and the meteor had a light curve expected for a single body with a peak emission at 100.4 km. The meteor's O I wake remained faint until a second event that was associated with a rapid exponential increase in brightness. Subsequently, the O I wake intensity followed the meteor's light curve closely and was fainter by only 2.8 magnitudes or a factor of 13 in intensity (Fig. 4, lower curve). In this regime, the meteor behaved as if due to a single solid body of a dimension corresponding to a peak intensity at an altitude of 106.0 km. When its mass was spent, the meteor intensity fell back to the original classical light curve, but with lower fraction of mass.

We interpret the light curve as follows: During the second fragmentation event (about frame 235), a fraction of the meteoroid mass may have broken into smaller fragments that were spent at about 100 km altitude. Part of those fragments may have been slowed down enough to support continuous ablation in the meteor afterglow. Small meteoroid fragments tend to be slowed relative to the larger fragments by collisions in the vapor cloud because of their larger surface-to-mass ratio. It is therefore significant that the afterglow was seen to form shortly after the second fragmentation event.

While fragmentation appears to cause meteor afterglow, even in relatively faint meteors, it is not necessarily the fragments that caused the gradual decay in light intensity. Secondary ablation is not always detected. It could be that fragmentation effectively contributed to thermalizing a larger volume of air plasma, and that it was the hot plasma that continued to excite the meteoric atoms.

The lack of atmospheric lines and bands in the bright fireball afterglow could mean that the air plasma is enriched in meteoric metals in the region contributing to the afterglow. There could also be a narrower zone near the center of the meteoroid's (or meteoroid fragment's) path than that from which the meteor emissions are observed.

The O I wake

In addition to the afterglow, there is also the oxygen green-line emission, a sensitive indicator

of atom density. The green line in natural airglow is caused by the catalytic recombination of oxygen atoms by meteoric metal atoms:

$$O + O + M \rightarrow O_2^* + M \quad (3)$$

$$O_2^* + O \rightarrow O\ (^1S) + O_2$$

The green-line intensity due to the $^1S \rightarrow {}^1D$ transition and, hence, is proportional to $[O]^3$, making this a sensitive indicator of O I density. Once in an excited state, the lifetime is 0.76 s (Baggaley, 1976). Jenniskens *et al.* (2000c) calculated that the initial dissociation of about 15% of the oxygen molecules explain the intensity of the O I green line emission in the persistent train of the Chippenham Leonid fireball. For a small meteoroid, the percentage of dissociated oxygen molecules would be much less because the oxygen atoms would be spread over the same volume that they are in larger meteoroids, resulting in very low volume densities. The green-line emission was observed to peak at ~0.4 s after the meteoroid and then quickly decayed. There was no O I emission in the meteor spectrum. Kinetic processes that control Reaction 3 may be responsible for the initial increase in O I green-line intensity, while diffusion of the oxygen atoms would have lowered the O I density and caused the subsequent decay.

IMPLICATIONS

Temperature decay in faint meteors

If meteoric vapor or debris was shielded from the impinging air flow or slowed down by favorable induced speed during fragmentation, then the material would have been decelerated less violently. This may enhance the survival of organic compounds. Whether this process is important for all small ~150-μm meteoroids at the peak of their mass influx curve depends on whether fragmentation occurs in a similar manner, or whether shielding can occur efficiently.

Small grains tend to have a short track and ablate at an altitude independent of a mass (but increasing with speed) of about 89 km. Their mean speed is 25 km/s (Taylor and Elford, 1998). While the gas cools from 4,100 K to 250 K, the collision frequency at that altitude increases from 2,000/s to 8,000/s. The ambient temperature is about 220 K. Cometary grains are thought to have very small ~0.1-μm subunits (Greenberg, 2000), so that abundant fragmentation is expected to occur even in grains 150 μm in diameter. Shielding, however, is less efficient for small grains because the vapor cloud is expected to be of similar size but less dense. We propose that even in small grains, fragmentation and the relatively larger vapor cloud will increase the effective volume of air being processed, leading to a more gradual cooling in the wake.

In an empirical approach, the expected duration of the afterglow (B) for smaller meteoroids is mostly a function of how rapidly the parameter D decreases with decreasing mass. D is not a function of B_o (that is, the amount of secondary ablation), or of the speed with which the meteoric plasma can be slowed down (nearly instantaneous). Rather, D is likely a function of the amount of air plasma that is being created. If so, D may be proportional to the mass loss for the given mass, altitude (air density), and speed: $dM/dt \sim m^{2/3}\ \rho_a\ V^3$ (McKinley, 1961). The mass loss rate of a typical ~150-μm grain at the peak of the mass influx curve is 8×10^{-4} times that of the −3 magnitude Leonid studied here, while the –13 magnitude Leonid (at 84 km) had a mass loss rate 4×10^4 times larger. If D behaves as a power law, $D \sim (dM/dt)^{-0.24}$ and $D = 100\ s^{-1}\ eV^{-1}$ for a 150-μm grain. If D behaves as a logarithmic function, then D is approximately $-3.8 \log (dM/dt)$ and $D = 30\ s^{-1}\ eV^{-1}$. If D is a linear or exponential function of dM/dt, then $D = 19\ s^{-1}\ eV^{-1}$ as measured for our Leonid. For an assumed $D = 100\ s^{-1}\ eV^{-1}$, the temperature decay is as shown by the dashed line in Fig. 5, marked by a question mark. With this choice, there remains an enhancement over the calculated trend of $T(t) \sim t^{-1/2}$ by Boyd (2000).

Organic chemistry in the meteor wake

In a CO_2-rich early Earth atmosphere, all of the CO_2 would have dissociated at 4,300 K to form oxygen atoms and CO (Jenniskens *et al.*, 2000a). These products, along with electrons, would have been the main reactive species in the air plasma. O_2 and O_3 would have formed in very low abundance. Hydrogen from the organic matter in the meteoroid may have contributed some amount of H and OH radicals.

In a combustion process, the efficiency of chemical processes depends on the generation

and propagation of free radicals. Indeed, O atoms are used to reduce hydrocarbon pollutants in gaseous industrial waste and on cleaning surfaces. In the case of hydrocarbons, complete molecular conversion will result in the formation of carbon dioxide and water. In that process many different reactions occur, some involving molecular oxygen and other compounds. In the presence of only O and CO, the possible chemistry is limited to C and H extraction reactions and oxygen insertion.

In the meteor phase, there are about 6×10^4 oxygen atoms relative to all meteoric metal atoms in a -3 magnitude Leonid (Jenniskens *et al.*, 2004a), or an O I density of about 5×10^{17} atoms/cm^3 at 100 km. For a ~150-μm meteoroid at 25 km/s the kinetic energy decreases by a factor of 4×10^{-7}. With O atoms spread out over the same volume, the density of O atoms generated by a ~150-μm meteoroid is only 2×10^{11} atoms/cm^3. Since the standard atmospheric background O I density at 100 km is about 2%, or 1.5×10^{12} atoms/cm^3, the meteor-induced contribution of oxygen atoms is quite small.

In a CO_2-rich early Earth atmosphere, each organic compound released from the meteoroid would have been bombarded about 2,000/s $\times$ 2% $\times$ 0.02 s = 0.8 times before the plasma had cooled to 1,800 K (after about 0.02 s). A similar number of collisions with CO would also be expected, as well as about 40 collisions with CO_2. The oxygen atoms would have reacted with organic compounds to make radicals, which could then react efficiently with other atmospheric compounds:

$$\text{R-CH} + \text{O} \rightarrow \text{R-C}\cdot + \text{OH} \qquad (4)$$

followed by:

$$\begin{aligned} \text{R-C}\cdot + \text{CO}_2 &\rightarrow \text{R}\cdot + 2\text{CO} \\ &\rightarrow \text{R-CO}\cdot + \text{CO} \\ &\rightarrow \text{R-C}{=}{=}\text{C}\cdot + \text{O}_2 \end{aligned} \qquad (5)$$

No collisions between organic compounds would be expected at this stage. If only a few percent of the collisions with air compounds were inelastic and led to chemical reactions (Öpik, 1958), even small organic molecules could survive this meteor phase, albeit with some chemical change.

In the wake of the meteor, these reactions would have been inhibited by the rapid decline of radical concentrations to ambient background levels and by the quenching of existing organic radicals. After the air plasma had cooled to 1,800 K, the oxygen atom abundance is expected to have quickly declined to the atmospheric background level if the plasma remained in LTE. In a low radical and high ultraviolet background, organic radicals would be removed by losing H and by reactions with atmospheric radicals, electrons, and ions. In today's Earth atmosphere, metal atoms help lower the O I abundance in the meteor column by facilitating catalytic reactions with ambient ozone.

Although radical chemistry does not normally involve activation energy barriers and is not temperature dependent, the frequency of collisions and the abundance of radicals and ions in the meteor wake over time is. This work provides the data needed to calibrate the conditions in the cooling plasma behind the meteoroid, from which detailed chemical modeling can be attempted, an effort outside the scope of this paper.

ACKNOWLEDGMENTS

The 2001 Leonid MAC was sponsored by NASA's Astrobiology ASTID and Planetary Astronomy programs. This work meets with objective 3.1 of NASA's Astrobiology Roadmap (Des Marais *et al.*, 2003).

ABBREVIATIONS

CCD, charge coupled device; HSI, high-speed imager; LTE, local thermodynamic equilibrium; MAC, Multi-Instrument Aircraft Campaign; UT, universal time.

REFERENCES

Baggaley W.J. (1976) The excitation of the oxygen metastable OI ('s) state in meteors. *Bull. Astron. Inst. Czechoslov.* 27, 173–181.

Baggaley, W.J. (1977) The velocity dependence of meteoric green line emission. *Bull. Astron. Inst. Czechoslov.* 28, 277–280.

Betlem, H., Jenniskens, P., Spurný, P., Docters van Leeuwen, G., Miskotte, K., Ter Kuile, C.R., Zarubin, P., and Angelos, C. (2000) Precise trajectories and orbits of meteoroids from the 1999 Leonid meteor storm. *Earth Moon Planets* 82-82, 277–284.

Borovička, J. and Jenniskens, P. (2000) Time resolved

spectroscopy of a Leonid fireball afterglow. *Earth Moon Planets* 82-83, 399–428.

Boyd, I.D. (2000) Computation of atmospheric entry flow about a Leonid meteoroid. *Earth Moon Planets* 82-83, 93–108.

Bronshten, V.A. (1983) *Physics of Meteoric Phenomena,* D. Reidel Publishing Co., Dordrecht, The Netherlands.

Ceplecha, Z. (1992) Earth influx of interplanetary bodies. *Astron. Astrophys.* 263, 361–366.

Ceplecha, Z., Borovička, J., Elford, W.G., ReVelle, D.O., Hawkes, R.L., Porubcan, V., and Simek, M. (1998) Meteor phenomena and bodies. *Space Sci. Rev.* 84, 327–471.

Chu, X., Liu A.Z., Papen, G., Gardner, C.S., Kelley, M., Drummond, J., and Fugate, R. (2000) Lidar observations of elevated temperatures in bright chemiluminescent meteor trails during the 1998 Leonid shower. *Geophys. Res. Lett.* 27, 1815–1818.

Des Marais, D.J., Allamandola, L.J., Benner, S.A., Deamer, D., Falkowski, P.G., Farmer, J.D., Hedges, S.B., Jakosky, B.M., Knoll, A.H., Liskowsky, D.R., Meadows, V.S., Meyer, M.A., Pilcher, C.B., Nealson. K.H., Spormann, A.M., Trent, J.D., Turner, W.W., Woolf, N.J., and Yorke, H.W. (2003) The NASA Astrobiology Roadmap. *Astrobiology* 3, 219–235.

Greenberg, J.M. (2000) From comets to meteors. *Earth Moon Planets* 82-83, 313–324.

Halliday, I. (1958a) Meteor wakes and their spectra. *Astrophys. J.* 127, 245–252.

Halliday, I. (1958b) Forbidden line of O I observed in meteor spectra. *Astrophys. J.* 128, 441–443.

Halliday, I., Mcintosh, B.A., Babadzhanov, B.P., and Getman, V.S. (1980) Orbit, chemical composition, atmospheric fragmentation of a meteoroid from instantaneous photos. In *Solid Particles in the Solar System*, edited by I. Halliday and B.A. McIntosh, D. Reidel Publishing Co., Dordrecht, The Netherlands, pp. 111–116.

Hawkes, R.L. and Jones, J. (1978) The effect of rotation on the initial radius of meteor trains. *Month. Not. R. Astron. Soc.* 185, 727–734.

Jenniskens, P. (1999) Activity of the 1998 Leonid shower from video records. *Meteoritics Planet. Sci.* 34, 959–968.

Jenniskens, P. (2001) Meteors as a vehicle for the delivery of organic matter to the early Earth. In *ESA-SP 495: Proceedings of the Meteoroids 2001 Conference,* ESA Publications Division, Noordwijk, The Netherlands, pp. 247–254.

Jenniskens, P. (2003) Leonid MAC near-real time flux measurements and the precession of comet 55P/Tempel-Tuttle. *ISAS-SP* 15, 73–80.

Jenniskens, P. and Russell, R.W. (2003) The 2001 Leonid Multi-Instrument Aircraft Campaign—an early review. *ISAS Rep. SP* 15, 3–15.

Jenniskens, P., de Lignie, M., Betlem, H., Borovička, J., Laux, C.O., Packan, D., and Krüger, C.H. (1998) Preparing for the 1998/99 Leonid storms. *Earth Moon Planets* 80, 311–341.

Jenniskens, P., Wilson, M.A., Packan, D., Laux, C.O., Krueger, C.H., Boyd, I.D., Popova, O.P., and Fonda, M. (2000a) Meteors: A delivery mechanism of organic matter to the early Earth. *Earth Moon Planets* 82-83, 57–70.

Jenniskens, P., Lacey, M., Allan, B.J., Self, D.E., and Plane, J.M.C. (2000b) FeO "Orange Arc" emission detected in optical spectrum of Leonid persistent train. *Earth Moon Planets* 82-83, 429–438.

Jenniskens, P., Nugent, D., and Plane, J.M.C. (2000c) The dynamical evolution of a turbulent Leonid persistent train. *Earth Moon Planets* 82-83, 471–488.

Jenniskens, P., Schaller, E.L., Laux, C.O., Schmidt, G., and Rairden, R.L. (2004a) Meteors do not break exogenous organic molecules into high yields of diatomics. *Astrobiology* 4, 67–79.

Jenniskens, P., Laux, C.O., Wilson, M.A., and Schaller, E.L. (2004b) The mass and speed dependence of meteor air plasma temperatures. *Astrobiology* 4, 81–94.

Kondrat'eva, E.D. and Reznikov, E.A. (1985) Comet Tempel-Tuttle and the Leonid meteor swarm. *Solar Syst. Res.* 19, 96–101.

Le Blanc, A.G., Murray, I.S., Hawkes, R.L., Worden, P., Campbell, M.D., Brown, P., Jenniskens, P., Correll, R.R., Montague, T., and Babcock, D.D. (2000) Evidence for transverse spread in Leonid meteors. *Month. Not. R. Astron. Soc.* 313, L9–L13.

Love, S.G. and Brownlee, D.E. (1993) A direct measurement of the terrestrial mass accretion rate of cosmic dust. *Science* 262, 550–553.

McCrosky, R.E. (1955) Fragmentation of faint meteors. *Astron. J.* 60, 170.

McKinley, D.W.R. (1961) *Meteor Science and Engineering,* McGraw-Hill, New York.

Murray, I.S., Hawkes, R.L., and Jenniskens, P. (1999) Airborne intensified charge-coupled device observations of the 1998 Leonid shower. *Meteoritics Planet. Sci.* 34, 949–958.

Öpik, E. (1958) *Physics of Meteor Flight in the Atmosphere,* Interscience, New York.

Oró, J. and Lazcano, A. (1997) Comets and the origin and evolution of life. In *Comets and the Origin and Evolution of Life,* edited by P.J. Thomas, C.F. Chyba, and C.P. McKay, Springer Verlag, New York, pp. 3–28.

Park, C. and Menees, G.P. (1978) Odd nitrogen production by meteoroids. *J. Geophys. Res.* 83, 4029–4035.

Ponnamperuma, C., ed. (1981) *Comets and the Origin of Life, Proceedings of the 5th College Park Colloquium on Chemical Evolution,* D. Reidel Publishing Co., Dordrecht, the Netherlands.

Popova, O.P., Sidneva, S.N., Shuvalov, V.V., and Strelkov, A.S. (2000) Screening of meteoroids by ablation vapor in high-velocity meteors. *Earth Moon Planets* 82-83, 109–128.

Spurný, P., Betlem, H., van 't Leven, J., and Jenniskens, P. (2000) Atmospheric behavior and extreme beginning heights of the thirteen brightest photographic Leonid meteors from the ground-based expedition to China. *Meteoritics Planet. Sci.* 35, 243–249.

Stenbaek-Nielsen, H.C., Hallinan, T.J., Wescott, E.M., and Fîppl, H. (1984) Acceleration of barium ions near 8000 km above an aurora. *J. Geophys. Res.* 89, 10788–10800.

Stenbaek-Nielsen, H.C. and Jenniskens, P. (2003) Leonid at 1000 frames per second. *ISAS SP* 15, 207–214.

Taylor, A.D. and Elford, W.G. (1998) Meteoroid orbital element distributions at 1 AU deduced from the Harvard

Radio Meteor Project observations. *Earth Planets Space* 50, 569–575.

Taylor, M.J., Gardner, L.C., Murray, I.S., and Jenniskens, P. (2000) Jet-like structures and wake in MgI (518 nm) images of 1999 Leonid storm meteors. *Earth Moon Planets* 82-83, 379–389.

Thomas, P.J., Chyba, C.F., and McKay, C.P., eds. (1997) *Comets and the Origin and Evolution of Life,* Springer Verlag, New York.

von Zahn, U. (2001) Lidar observations of meteor trails: Evidence for fragmentation of meteoroids and their subsequent differential ablation. In *ESA SP-495*: *Proceedings of the Meteoroids 2001 Conference*, ESA Publications Division, Noordwijk, The Netherlands, pp. 303–314.

Address reprint requests to:
Dr. Peter Jenniskens
Center for the Study of Life in the Universe
SETI Institute
2035 Landings Drive
Mountain View, CA 94043

E-mail: pjenniskens@mail.arc.nasa.gov